European Journal of
Physical Sciences
(EJPS)

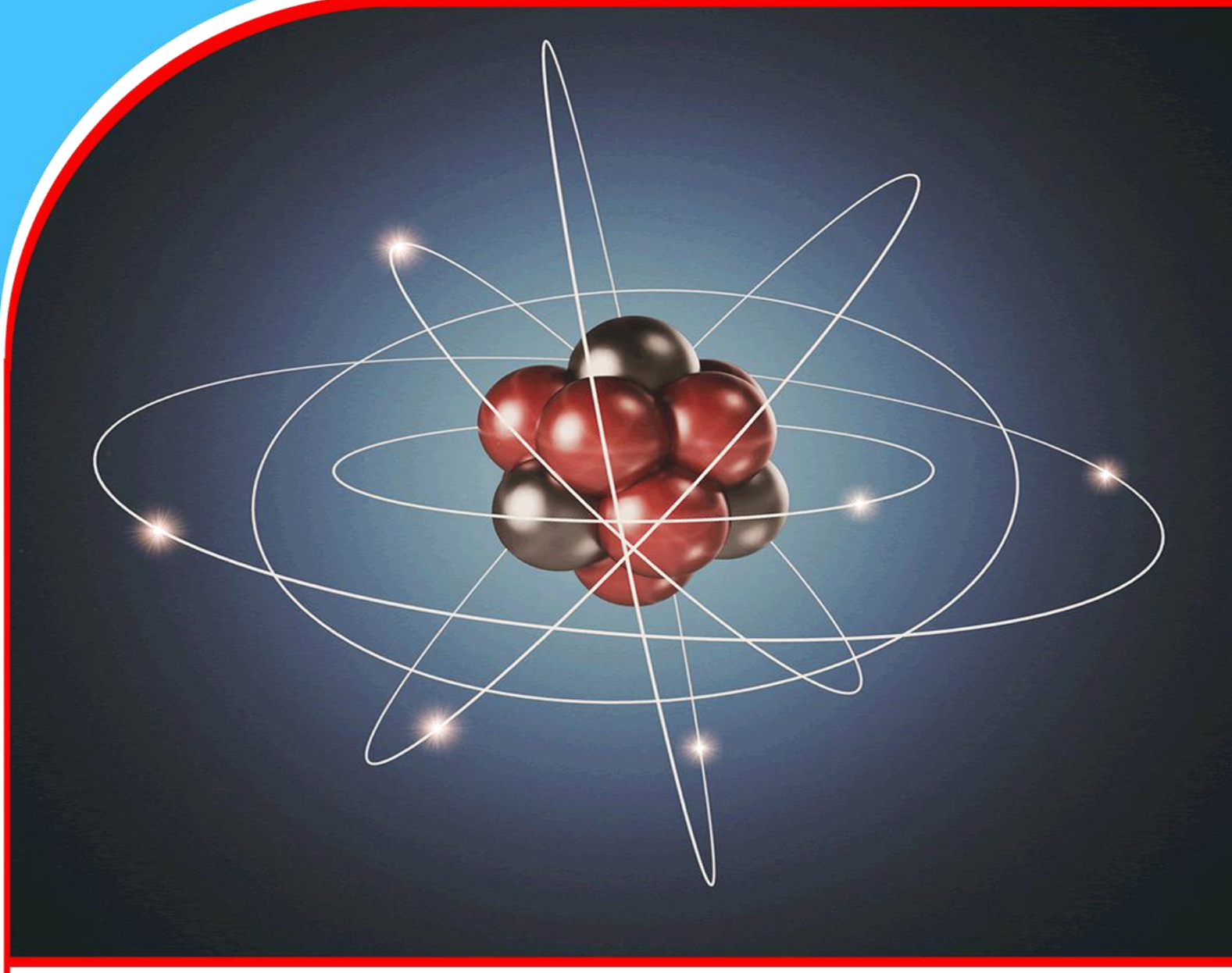

Improve the Performance of Perovskite-Based Solar Cells Using Buffer Layers and Reflective Layers by Simulation Software SCAPS-1D

Muaamar A. Kamil

European Journal of physical Sciences
ISSN 2788-8223 (Online)
Vol.8, Issue 1, pp 10 - 28, 2025
www.ajpojournals.org

Improve the Performance of Perovskite-Based Solar Cells Using Buffer Layers and Reflective Layers by Simulation Software SCAPS-1D

Muaamar A. Kamil[1*]
Department of physics, College of Education for pure science, Tikrit University, Tikrit, Iraq

Article history
Submitted 14.12.2024 Revised Version Received 10.01.2024 Accepted 01.02.2025

Abstract

Purpose: This study aims to improve the performance of perovskite FAPbI 3 (formamidinium tri-iodide)-based solar cells by modifying some of the solar cell layers.

Materials and Methods: In this research SCAPS 1-D program was relied upon in the approved solar cell simulation which is a computer software used to simulate one-dimensional solar cell designed at the University of Gent Electronics and Information Systems in Belgium.

Findings: In this study, suitable buffer layers were added, which led to an improvement in the cell's output .The best buffer layer was STO, which gave the best results of η (27.34%), VOC (1.30V), JSC (28.35 mA/cm 2), and FF (73.66%). Then the back reflection layer was changed. An increase in open-circuit voltage, short-circuit current, and fill factor was observed. The layer consisting of CuScN (copper selenium nitride) gave the best results of JSC (28.35 mA/cm 2), VOC (1.45 V), FF (75.85%), and conversion efficiency η (31.21%). Subsequently, a second absorbing layer was added to the cell between the reflection layer and absorbing layer, leading to an increase in the solar cell's conversion efficiency. The layer that gave the best results was Sb2Se3 (antimony selenide), achieving JSC (38.71 mA/cm 2), VOC (1.45 V), FF (78.45%), and conversion efficiency (44.29%).

Implications to Theory, Policy and Practice: The compounds (CdS,STO,TiO2,V2O5,WS2,ZnO) can be used as a buffer layer with a power gap between (1.8-3.3 eV) and have a suitable interface for the FAPbI3- based solar cell.

Keywords: *Solar Cell, Buffer Layer, Fapbi3, Reflection Layer, Scaps-1D, Converter Efficiency*

INTRODUCTION

The urgent need to find high-performance and low-cost materials for photovoltaic applications led researchers to undertake a new study Absorption Materials for Solar Cell Applications. Materials used to manufacture perovskite solar cells have notable characteristics such as high optical absorption capability [1]. Long electron- hole length, low binding strength of exciton, high energy conversion efficiency (PCEs), which is easy to process. [2,3]. To the date, the PCE of PSCs has been reached from 3.1 % to 25.7 % for the single junction and to 31.3 % for the tandem architecture [4]. Due to those traits, PSCs have become a research Point of attraction in the field of photovoltaics. Some studies have found PCEs of PSCs as high as 25.5% [5], which can be compared to silicon-based solar cells and indicate wide development possibilities of PSCs. The perovskite solar cell based on formamidinium tri-iodide (HC(NH2)2PbI3 or FAPbI3) achieved high thermal stability [6].

Moreover, FAPbI3 has an energy gap of 1.48 eV, which is more suitable for capturing the solar spectrum [7]. In recent years, studies on the perovskite layer are mainly focused on the formamidinium lead iodide phase (FAPbI3) because it has along carrier lifetime and wide absorption range to enhance the open circuit voltage (VOC) and short circuit current density (JSC) of PSCs [8,9]. Besides, the exploitation of the monocrystalline device with very low defect density was also reported to achieve high performance PSCs. Charge transport layers (HTL &ETL) have great effect of enhancing PCE during extraction of holes (h +) from absorption layer and electron generation (e−).

To achieve best PSC performance, a suitable combination of available electron transfer material (ETL) and holes transport material (HTL) should be checked along with the absorption layer. The recently widely used HTL is spiro OMeTAD of organic nature [10]. Back reflection layer where it works to reflect the photons that pass-through Absorption layer increases concentration of charge carriers and reduces recombination, increases the photon current [11]. The main role of the buffer layer in solar cells with absorption layer (FAPbI3) is to form an interstitial surface with the absorption layer, and connect maximum light to the absorption layer area [12]. This layer must have less of a loss of absorption and be able to take out the light current carriers created using minimal recombination losses, and transfer them to the outer circuit with minimal electrical resistance. To obtain high-performance photovoltaic cells with minimal loss of resistance, the energy gap of the buffer layer is better high in order to allow the passage of the maximum load carriers to the absorbing layer, which should improve the buffer layer because it aligns the energy gap between the absorption layer and the window layer [13]. This research addresses comparing the cell practically manufactured by the researcher and theoretically comparing it after inserting all the parameters used in its design into the SCAPS program, in order to determine the credibility of the simulation program. Thus, the theoretical cell was improved by adding ETL buffer layers and BSL reflective layers thereafter, adding a second absorption layer between the reflection layer and the absorption layer and studying the extent to which it affected the solar cell's performance.

Modeling

Numerical Simulation in SCAPS-1D

In this research SCAPS 1-D program was relied upon in the approved solar cell simulation which is a computer software used to simulate one-dimensional solar cell designed at the University of Gent Electronics and Information Systems in Belgium. Through the SCAPS 1-D program, the

characteristics of the solar cell consisting of seven layers can be obtained as a maximum and know the thickness, vaccination and defects and their impact on the work of the cell and obtain the characteristics of the current-voltage (I-V)and characteristics (C-V)and quantitative efficiency (QE)as well as properties (C-F) as well as solar spectrum type can be selected (multiple spectrums or single spectrum) Store and load all cell settings and can by SCAPS 1-D program draw curves like curve (I-V) and (QE) [14]. as well SCAPS 1-D can solve the Poisson equations and continuity in semiconductors and uses the Newton- Irvson method, carrier transport equations and two drift current and diffusion intensity equations. We start by writing the Poisson equation: [15]

$$\nabla(E) = \frac{q}{\varepsilon}(p - n + N^{+} - N^{-}) \ldots\ldots\ldots\ldots\ldots\ldots\ldots\ldots.1$$

D A

where E represent the electrical field, q represent is elementary charge, ε represent is permittivity of the absorber, n(p) represent is density of electrons (holes), and ND (NA) is donor (acceptor) concentration. Then, we can write the continuity equations for electrons and holes by equation:[16]

$$\frac{dn}{dt} = \frac{1}{q}(\nabla(J_n) + G_n - R_n \ldots\ldots\ldots\ldots\ldots\ldots\ldots\ldots.....2$$

$$\frac{dp}{dt} = q(\nabla(J_p) + G_p - R_p \ldots\ldots\ldots\ldots\ldots\ldots\ldots\ldots\ldots..3$$

Where G_n (Gp) is electron (hole) generation rate, J_n (J_p) is electron (hole) current density, and R_n (Rp) is electron (hole) recombination rate.

Finally, the charge carrier equations for the density of diffusion current and drift can be obtained from the following equations [17].

$$J_n = q(\mu_n nE + D_n \nabla n) \ldots\ldots\ldots\ldots\ldots\ldots\ldots\ldots\ldots\ldots..4$$

$$J_p = q(\mu_p PE + D_p \nabla p) \ldots\ldots\ldots\ldots\ldots\ldots\ldots\ldots\ldots\ldots..5$$

where μn (μp) is electron (hole) mobility and D is the diffusion coefficient.

Through solar cell output, the cell's work can be recognized and distinguished from the rest of the solar cell and consists of four outputs It is the voltage of the open circuit (V_{OC}) and the short current circuit (J_{SC}) fill factor (FF) from which the efficiency of the solar cell can be determined (η) and the current passing through the cell is given the following relationship [18].

$$I = I_{\circ}\left[exp\left(\frac{qv}{KT}\right) - 1\right] - I_L \ldots\ldots\ldots\ldots\ldots\ldots\ldots\ldots\ldots\ldots\ldots\ldots\ldots\ldots\ldots\ldots\ldots\ldots 6$$

Where K is the Boltzmann constant, T is the temperature measured in Kelvin, (I) Current of load and (I_L) the luminescence current. To calculate the open circuit voltage (Voc) which is at its highest value when the current is zero and according to the following equation.

KT L_I KT L_I

$$V_{OC} = \frac{Ln}{q}\left(\frac{}{1} - 1\right) \approx \frac{Ln}{q}\left(\frac{}{I_\circ}\right) \ldots\ldots\ldots\ldots\ldots\ldots 7$$

Where (I_O) is the reverse saturation current and is calculated from the following equation.

$$I_o = DT^3 \exp\left[-\frac{E_g}{KT}\right] = A\left[\frac{qD_e n^2}{L_e N_A} + \frac{qD_h n^2}{L_h N_D}\right] \ldots\ldots\ldots 8$$

Where Eg the energy gap, (Le, Lh) length of diffusion of electrons and holes, A cross- sectional aera of the diode. The relationship between the open circuit voltage and the short circuit current is given by the following equation.

$$I_{SC} = I_\circ\left[e^{qV_{OC}/KT} - 1\right] \ldots\ldots\ldots\ldots\ldots\ldots\ldots\ldots\ldots\ldots 9$$

The filling factor is the ratio between maximum electrical power and maximum current and voltage density that can be generated by the cell. fill factor can be calculated by following equation.[19]

$$FF = \frac{P_{max}}{P_t} \ldots\ldots 10$$

Solar cell efficiency can be calculated from the following relationship:

$$\eta = \frac{P_m}{P_t} = \frac{V_{oc}.J_{sc}.FF}{P_t} \ldots\ldots\ldots\ldots\ldots\ldots\ldots\ldots\ldots\ldots\ldots 11$$

quantum efficiency is inversely proportional with wavelengths, depending on the equation (12).

$$Q_E = 1.24\frac{R_\lambda}{} \ldots\ldots\ldots\ldots\ldots\ldots\ldots\ldots\ldots\ldots\ldots\ldots\ldots 12$$

FF Fill factor, η cell efficiency, J_{sc} short-circuit current, V_{oc} open circuit voltage, V_{max} maximum voltage, I_{max} maximum current, P_{max} maximum power, P_{in} input power (Rλ) represents the responsive of back surface layer, (λ) the wavelength [20].

Solar Cell Structure

The solar cell structure is composed of (glass / ITO / SnO_2 / $FAPbI_3$ / Spiro-OMeTAD /Au) as shown in figure 1. ITO is the window layer of transparent metal oxides and has a relatively large energy gap of about (3.6 eV). Then, the buffer layer SnO_2 has a suitable energy gap and it works on tuning between the absorption layer and the window, which is at a limit (3.6 eV) [7].

Then comes the $FAPbI_3$ absorption layer, which has a relatively small energy gap that has about (1.5 eV). Then it is followed bake reflection layer Spiro-OMeTAD and it has energy gap an about (2.9 eV) [21]. also, this cell has an ohmic front contact and back Schottky gold contact with work function of the about of (5eV) [22]. And we also do not forget that the cell is deposited on the ground from glass and figure (1) showed the structure of the solar cell. Table (1) shows the values of the parameters that were entered in the program to study theoretical cell performance and compare it with the experimental side of the parent cell [23].

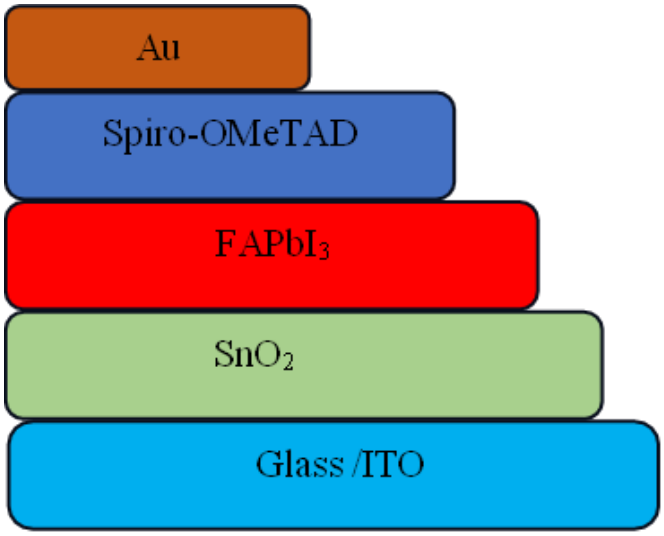

Figure 1 Device Structure

Table 1 Cell Parameters Comparable Theoretically

Parameters	symbol (unit)	ITO [24,25]	SnO2[26,27]	FAPbI3 [7]	Spiro-OMeTAD [28,29]
Thickness	W(µm)	0.100	0.100	0.800	0.300
Bandgap	Eg (eV)	3.6	3.6	1.5	2.9
Electron affinity	χ (eV)	4.100	4.500	4	2.2
Dielectric permittivity	ϵr	10.000	9	6.6	3
CB effective density of states	$N_C(cm^{-3})$	2.200 E+18	2.200 E+18	1.200 E+19	2.500 E+20
VB effective density of states	$N_V(cm^{-3})$	1.800 E+19	1.800 E+19	2.900 E+18	2.500 E+20
Electron thermal velocity	V_n(cm/s)	1.000 E+ 7	1.000 E+ 7	1.000E+ 7	1.000E+ 7
Hole thermal velocity	V_P(cm/s)	1.000 E+ 7	1.000 E+ 7	1.000E+ 7	1.000E+ 7
Electron mobility	$\mu_n(cm^2/v.s)$	1.000 E+ 2	1.000 E +2	2.700 E+0	2.100 E-0
Hole mobility	$\mu_p(cm^2/v.s)$	2.500E+18	2.500 E+19	1.800 E+0	2.600 E-3
Shallow uniform donor density	ND $(1/cm^3)$	1.000 E+18	5.000 E+19	0	0
Shallow uniform acceptor density	NA $(1/cm^3)$	0	0	1.000 E+18	1.000 E+18

FINDINGS

Comparing Experimental Cell Results with Theoretical Results

The experimental results of the cell were matched with the simulation results in the beginning to ensure the reliability of the simulation program, simulation was done for practical research [23] with the theoretical results was performed was done using SCAPS-1D software. The results showed a high match between the practical and theoretical aspect and this is shown in Table 2.

Table 2 A Comparison Between the Experimental and Theoretically

No	Solar cell	VOC (V)	JSC (mA/cm^2)	FF%	η%
1	(experimental)	1.01	21.65	75.27	16.6
2	(theoretical)	1.04	21.75	72.88	16.6

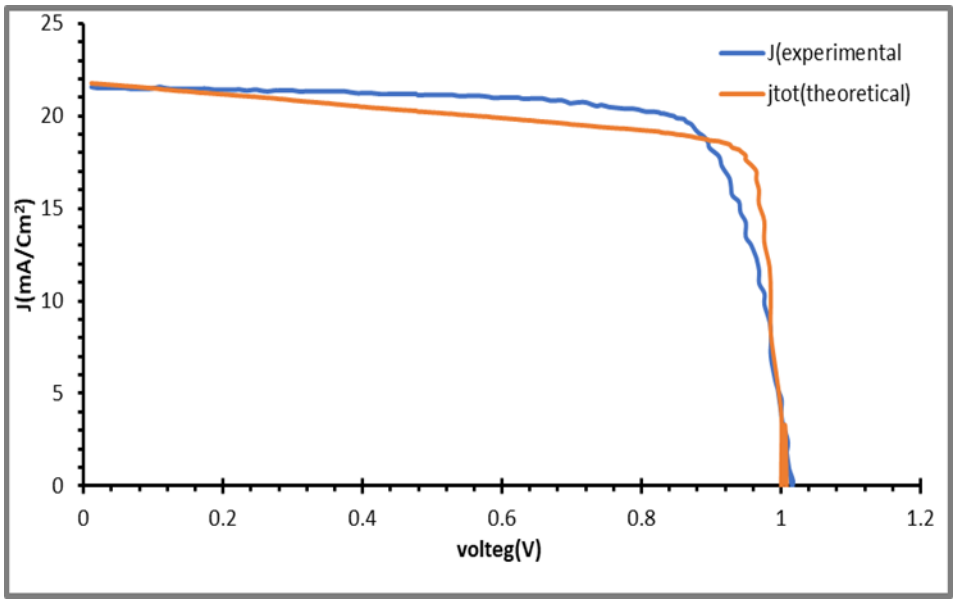

Figure 2 Curved I-V For Experimental and Theoretical Work

Impact of Adding Different Buffer Layer

The main role of buffer layer in the solar cells with absorption layer ($FAPbI_3$) is to form an interface with the absorption layer. It allows passage maximum amount of light to absorption layer [30]. This layer should be minimal absorption loss and be able to take out the light current carriers created using minimal re-union losses. and transported to the outer circle with minimal resistance, it is preferable that the energy gap of the buffer layer be high in order to allow the passage of the greatest number of carriers to the absorbing layer, which should improve the buffer layer because it aligns the energy gap between the absorption layer and the window layer [31]. The compounds (CdS,STO,TiO_2,V_2O_5,WS_2,ZnO) can be used as a buffer layer with a power gap between (1.8-3.3 eV) and have a suitable interface for the $FAPbI_3$- based solar cell. Table (3) shows the values of the parameters of the buffer layer used in the simulation. Solar cells with $FAPbI_3$ composition were studied with different layers of alignment for best solar cell performance, where an improvement in output values (Voc, Jsc, FF, eta) was observed, and we note that there is a discrepancy in values as the best values we obtained are using the compound (STO) that improved the interface with the absorption layer, where it possesses an energy gap (3.2 eV). Table (4) shows the cell output values after adding the buffer layers. Figure (4) shows the extent to which the voltage and current curve is affected after adding buffer layers to replace the (SnO_2) layer in the original cell. Figure (4) represents the energy levels of the cell (glass / ITO / STO / $FAPbI_3$/ Spiro-OMeTAD / Au) that gave the best results. Figure (5) shows the energy levels of the cell (glass/ITO/V_2O_5/$FAPbI_3$/Spiro- OMeTAD /Au) that gave the lowest level of conversion efficiency.

Tabel 3 Parameters of the Buffer Layer Used in the Simulation Solar Cells

Parameters	symbol (unit)	CdS [32,33]	STO [34,35]	TiO2[52]	ZnO [35]	V2O5 [36]	WS2 [37-39]
Thickness	W(µm)	0.100	0.100	0.100	000.1	0.100	0.100
Bandgap	Eg (eV)	2.4	3.2	3.2[53]	3.3	2.3	1.8
Electron affinity	χ (eV)	4.200	4	4[53]	4.45	3.99	3.9
Dielectric permittivity	ϵr	9.000	8.7	10[53]	9	4.28	13.6
CB effective density of states	$(cm^{-3})N_C$	1×10^{18}	1.7×10^{19}	2×10^{19}	2×10^{18}	2.2×10^{18}	$2.\times10^{18}$
VB effective density of states	$(cm^{-3})N_V$	1×10^{19}	2×10^{20}	2.5×10^{18}	1.8×10^{19}	1.8×10^{19}	2×10^{20}
Electron thermal velocity	(cm/s)V_n	1×10^{7}	1×10^{7}	1×10^{7}	1×10^{7}	1×10^{7}	1×10^{7}
Hole thermal velocity	(cm/s)V_P	1×10^{7}	1×10^{7}	1×10^{7}	1×10^{7}	1×10^{7}	1×10^{7}
Electron mobility	$(cm^2/v.s)\mu_n$	5 0	5.3×10^{3}	5 0	1×10^{2}	1.26	1×10^{2}
Hole mobility	$(cm^2/v.s)\mu_p$	20	6.6×10^{2}	50	25	34.5	1×10^{2}
Shallow uniform donor density	ND $(1/cm^3)$	1×10^{15}	2×10^{18}	1×10^{17}	1×10^{18}	1×10^{17}	1×10^{17}
Shallow uniform acceptor density	NA $(1/cm^3)$	0	0	0	0	0	0

Table 4: Output Values of the Solar Cell After Adding the Insulating Layers

Materials	VOC(V)	JSC (mA/cm^2)	FF %	η%
CdS	1.28	28.37	73.13	26.73
STO	1.30	28.35	73.66	27.34
TiO2	1.30	28.35	73.61	27.19
V2 O5	1.16	21.53	73.44	18.35
WS2	1.30	28.33	73.67	27.31
ZnO	1.30	28.36	73.67	27.33

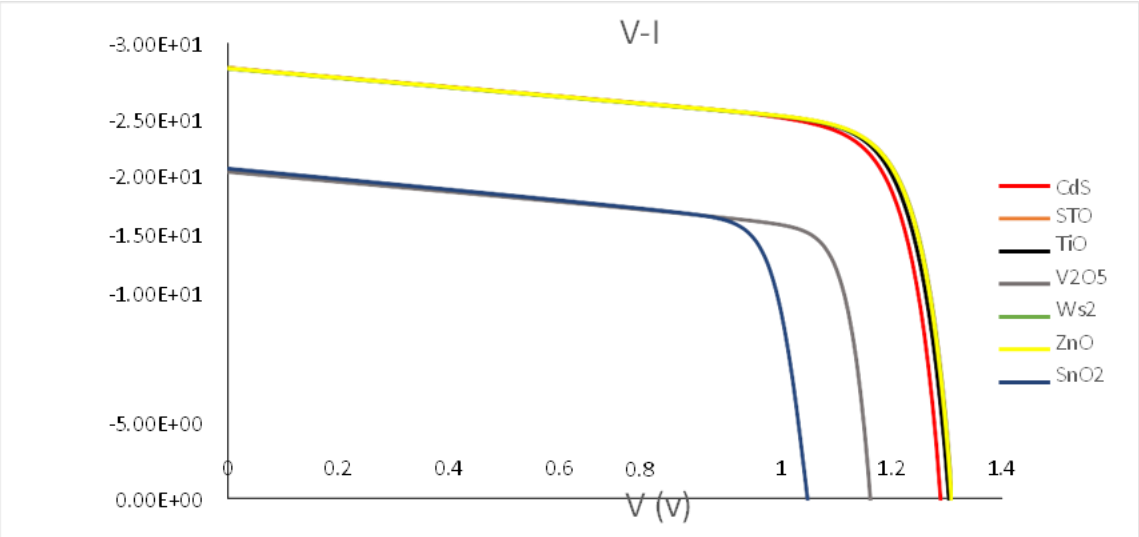

Figure 3 Curve I-V After Changing Buffer Layer and with (Sno2)

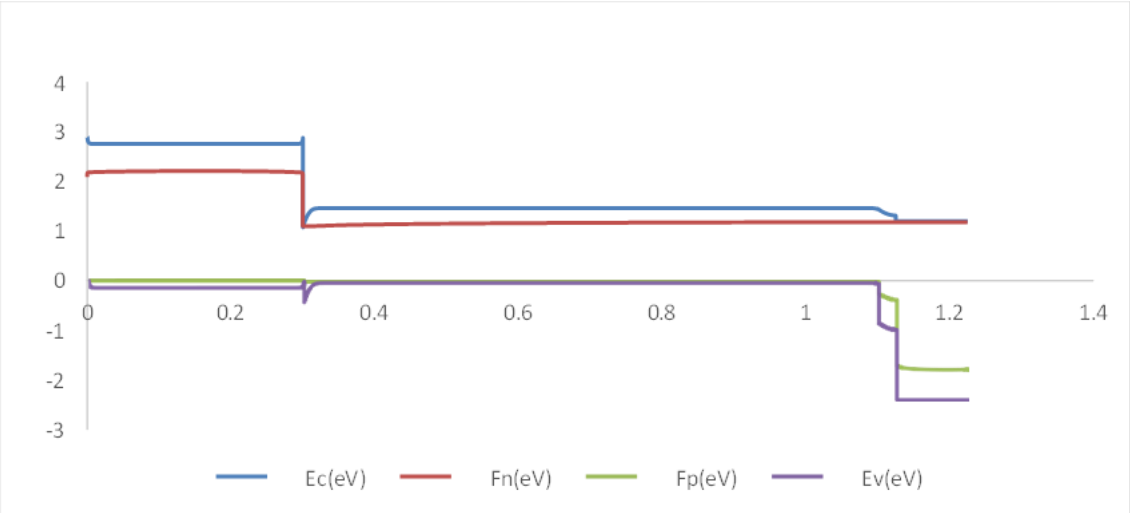

Figure 4 Energy Band of the Cell (Glass / ITO / STO / Fapbi3/ Spiro-Ometad / Au)

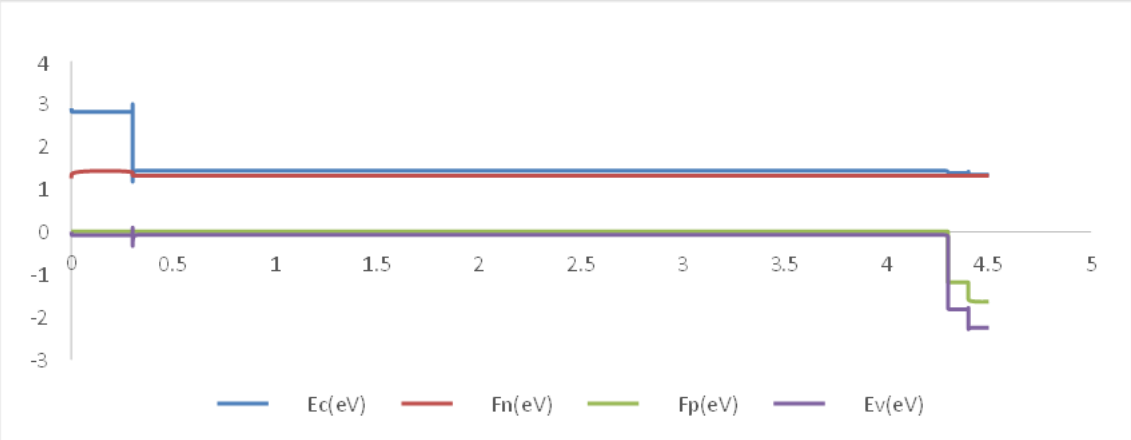

Figure 5 Energy Band of the Cell (Glass / ITO / V2O5 / Fapbi3/ Spiro-Ometad / Au)

Figure (6) illustrates the quantum efficiency (QE%) of the optimized cells compared to the original cell. It is observed that the change occurs within the confined range of 350 nm to 850 nm. This change is attributed to the energy gap of the buffer layers, which ranges from 1.8 eV

to 3.3 eV, as described by equation (12). In other words, the buffer layers are transparent to wavelengths greater than 850 nm, allowing a higher number of photons to be absorbed by the absorption layer [40].

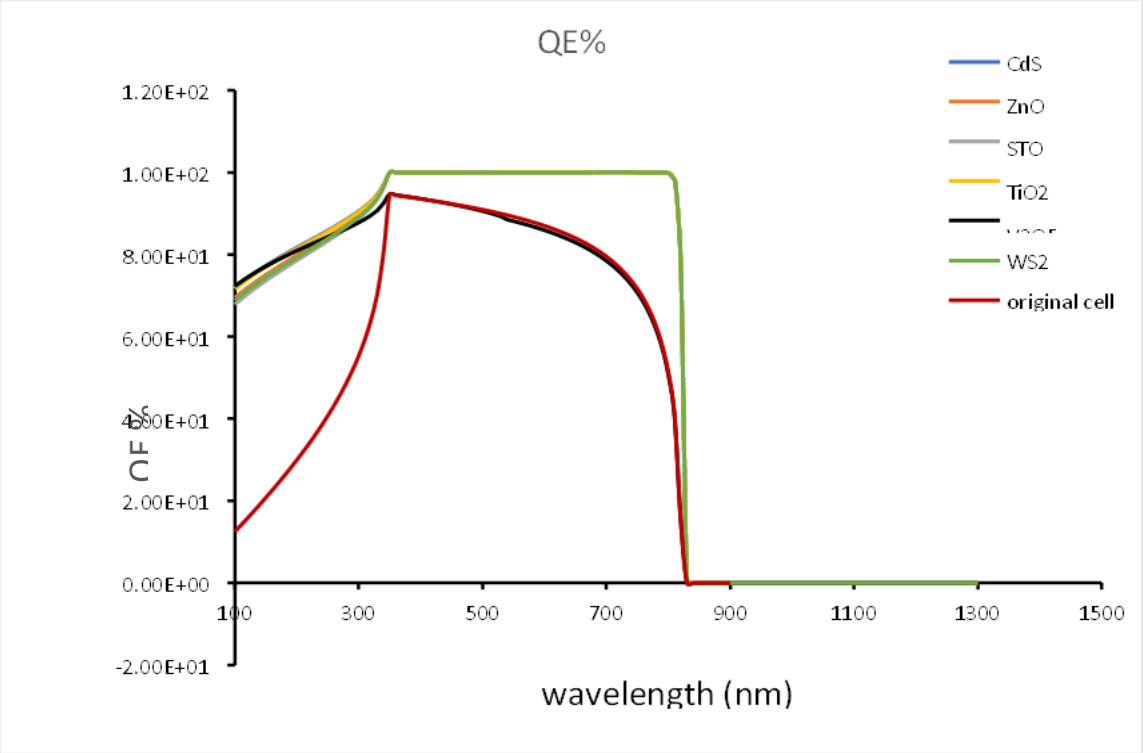

Figure 6 Wavelength Relation with Quantum Efficiency for Different Buffer Layer with Original Cell

Impact Adding a Back Surface Layer (BSL)

After changing the original cell buffer layers and selecting the layer that gave the best results is the STO layer ((glass/ITO/STO/FAPbI3/ Spiro-OMeTAD /Au)), we will study the effect of adding Various outer layer (BSL) with the following chemical compositions (CuO,CdTe, CuScN, PEDOT: PSS, MoSe2,MoS2), cell parameters for absorption, and buffer and window layers constant. Table (5) shows the parameters of the back surface layer, where the best BSL was shown to be the CuScN, due to the low energy gap which reduces the height of the potential barrier and reduces the recombination of minority carriers upon back contact where it is evident that the effect of these layers on the cell will increase exchange efficiency and fill factor, as the surface layer reflects photons to the absorption layer, increases the number of charge carriers and reduces the recombination of the surface layer thus making the connection more ohmic and conducting the photo-current high [41]. Figure (7) shows the current-voltage curves and Table 6 shows the outputs of the improved cell after adding the different reflection layers.

Table 5 The Physical Parameters of the Back Surface Layer (BSL)

Parameters	symbol (unit)	CdTe [42]	CuO [43]	CuCSN [44]	MoSe2 [43]	MoS2[45]	PEDOT: PSS [46]
Thickness	W(µm)	0.100	0.100	0.100	000.1	0.100	0.100
Bandgap	Eg (eV)	1.4-1.9	2.1	3.4	1.3	2.3	1.8
Electron affinity	χ (eV)	4.28	3.2	1.9	4.32	3.99	3.9
Dielectric permittivity	ϵ_r	9.4	7.11	10	7.29	4.28	13.6
CB effective density of states	$(cm^{-3})N_C$	7.5×10^{17}	2.2×10^{20}	1.7×10^{19}	9×10^{17}	2.2×10^{18}	2×10^{18}
VB effective density of states	$(cm^{-3})N_V$	1.8×10^{19}	5.5×10^{19}	2.5×10^{18}	9×10^{20}	1.8×10^{19}	$2. \times 10^{20}$
Electron thermal velocity	(cm/s)V_n	1×10^{7}	1×10^{7}	1×10^{7}	1×10^{7}	1×10^{7}	1×10^{7}
Hole thermal velocity	(cm/s)V_P	1×10^{7}	1×10^{7}	1×10^{7}	1×10^{7}	1×10^{7}	1×10^{7}
Electron mobility	$(cm^2/v.s)\mu_n$	500	3.4	1×10^{-4}	2×10^{-2}	1.26	1×10^{2}
Hole mobility	$(cm^2/v.s)\mu_p$	60	3.4	1×10^{-1}	2×10^{-4}	34.5	1×10^{2}
Shallow uniform donor density	N_D $(1/cm^3)$	0	0	0	0	0	0
Shallow uniform acceptor density	N_A $(1/cm^3)$	1×10^{21}	1×10^{18}	1×10^{18}	1×10^{18}	1×10^{17}	1×10^{17}

Table 6 Shows the Results Obtained When Adding a Back Surface Layer

Materials	**VOC (V)**	**JSC(mA/cm²)**	**FF %**	**η%**
CuO	1.4	28.35	75	30.47
CdTe	1.18	28.35	78.96	26.62
CuScN	1.45	28.35	75.85	31.21
PEDOT: PSS	1.36	28.35	73.45	28.51
MoSe2	1.12	28.18	78.62	24.92
MoS2	1.11	28.35	78.96	24.95

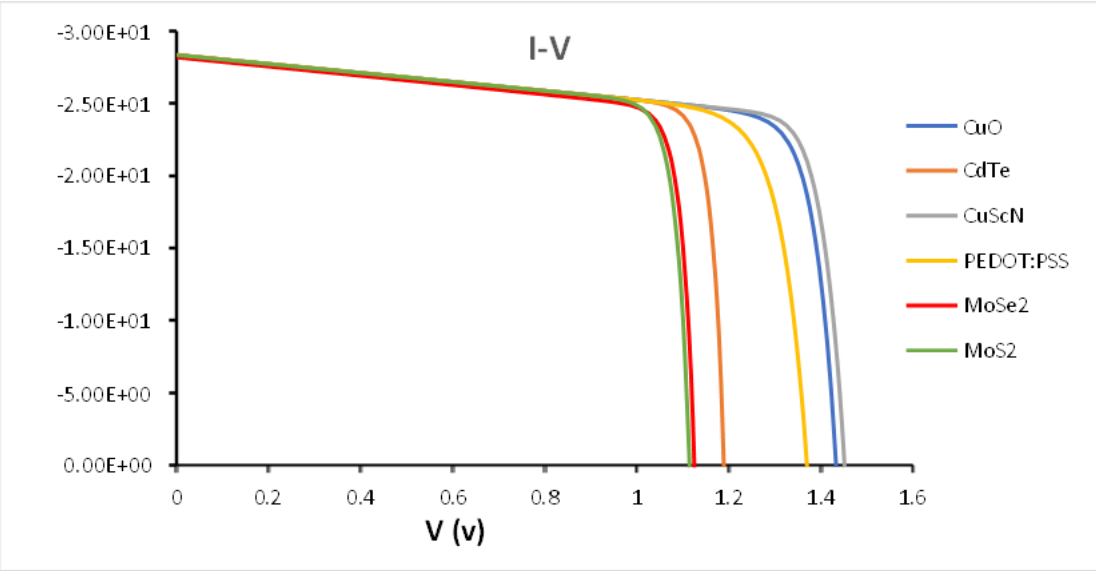

Figure 7 Current-Voltage Curves after Adding Different BSL Layer

To assess the impact on quantum performance (QE), defined as the quantity of electron-hole pairs generated in response to incident light on the solar cell, Figure 8 illustrates the QE values before and after reintroducing surface layers to the cell. The quantum efficiency of the system demonstrates a significant progression, starting at 57% at a wavelength of 300 nm and gradually increasing to 100% at 350 nm. This observed trend is attributed to the pronounced absorption of photons from the reflection layer, particularly those with longer wavelengths. It is noteworthy that the quantum efficiency bears a resemblance to the square [47]. The optimal for solar cell operation involves performance followed by a gradual decrease in efficiency, ultimately reaching zero at the wavelength of (850nm). This decline can be attributed to the low diffusion length and the fact that absorption becomes zero at longer wavelength. Regarding the cell prior to the reintroduction of surface layers, it is observed that the quantum efficiency curve starts to decrease at the wavelength (380nm) and continues until it reaches zero at the wavelength (850nm).

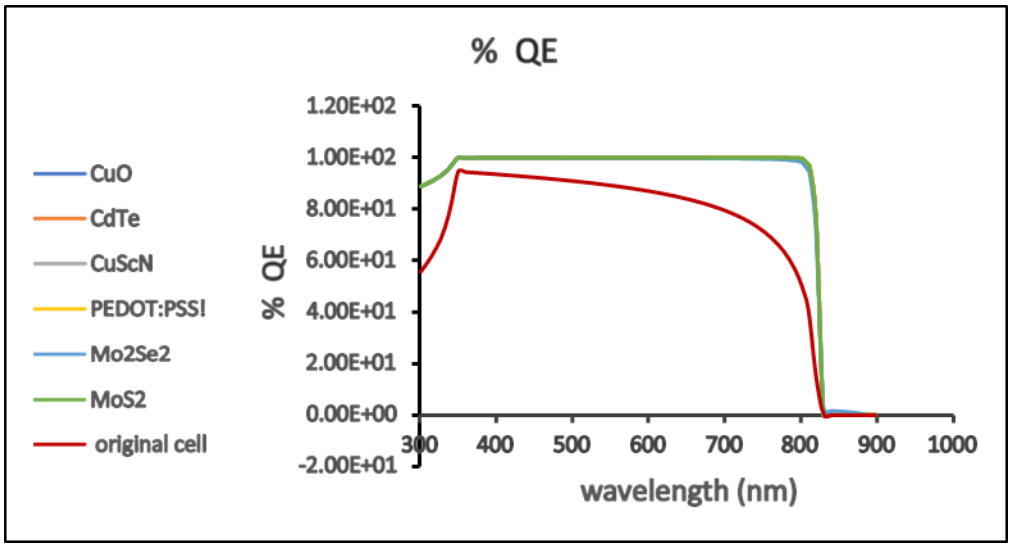

Figure 8 Wavelength Relation with Quantum Efficiency for Different BSL Layer with Original Cell

Effect of Adding a Second Absorbing Layer

In order to enhance the performance and efficiency of the optimized solar cell, we will study the addition of absorption layers to the cell and evaluate their impact on its performance. Among these absorption layers are CsPbI3, CsSnI3, (FA)2BiCuI6, FASnI3, Sb2Se3. Table7 illustrates the parameters for the absorption layers that have been added, showing that incorporating these layers into the optimized cell will increase the conversion efficiency and enhance the fill factor. This is achieved by increasing the concentration of charge carriers, reducing surface recombination, and improving the contact interface. Consequently, the photocurrent increases, leading to improved cell performance and I-V characteristics. Table 8 presents the obtained results when adding the absorption layer to the optimized. The best absorption layer that provided the highest values is Sb2Se3, located between the original absorption layer and the reflective layer. The thickness of both the original absorption layer and the added absorption layer is 2µm. Figure 10 shows curved voltage current after adding second absorption layers for optimized solar cell. It is observed that the best absorption layer added to the cell is Sb2Se3, which achieved the highest conversion efficiency of 44.29% (η), a fill factor (FF) of 78.45%, a short-circuit current (JSC) of 38.71 (mA/cm^2), and an open-circuit voltage (VOC) of 1.45 (V).

Table 7 Optimized Cell Added Absorption Layer Parameters

Parameters	symbol (unit)	CsPbI3 [48]	CsSnI3 [49]	(FA)2BiCuI6 [50]	FASnI3 [51]	Sb2Se3 [43]
Thickness	W(µm)	2.000	2.000	2.000	2.000	2.000
Bandgap	Eg (eV)	1.69	1.3	1.55	1.4	1.2
Electron affinity	χ (eV)	3.95	3.7	3.7	3.52	4.04
Dielectric permittivity	ϵr	6	25	5.27	8.2	18
CB effective density of states	N_C (cm^{-3})	1.1 x10^{+20}	1.4 x10^{+19}	1 x10^{+22}	1x10^{+18}	2.2x10^{+18}
VB effective density of states	N_V (cm^{-3})	8.2 x10^{+20}	1.4 x10^{+18}	1 x10^{+21}	1x10^{+18}	1.8 x10^{+19}
Electron thermal Velocity	V_n(cm/s)	1 x10^{+7}	1 x10^{+7}	1 x10^{+7}	1 x10^{+7}	1 x10^{+7}
Hole thermal velocity	V_P(cm/s)	1.0 00 E +7	E 1.000 +7	E 1.000 +7	E 1 +7	1.000 +7
Electron mobility	μ_n (cm^2/v.s)	25	0.6	2	22	1 1.5 x10^{+1}
Hole mobility	μ_p (cm^2/v.s)	25	42	1	22	5.10
Shallow uniform donor density	ND (1/cm^3)	0	0	0	0	0
Shallow uniform acceptor density	NA (1/cm^3)	1x10^{+15}	1x10^{+17}	1x10^{+16}	7x10^{+16}	1.13x10^{+17}

Table (8) Cell Output After Adding Absorption Layers for Improved Cell

Materials	VOC (V)	JSC (mA/cm^2)	FF %	η%
CsPbI3	1.45	28.14	75.76	30.93
CsSnI3	1.46	35.48	78.11	40.58
(FA)2BiCuI6	1.45	28.16	75.56	30.76
FASnI3	1.45	31.45	76.56	35.11
Sb2Se3	1.45	38.71	78.45	44.29

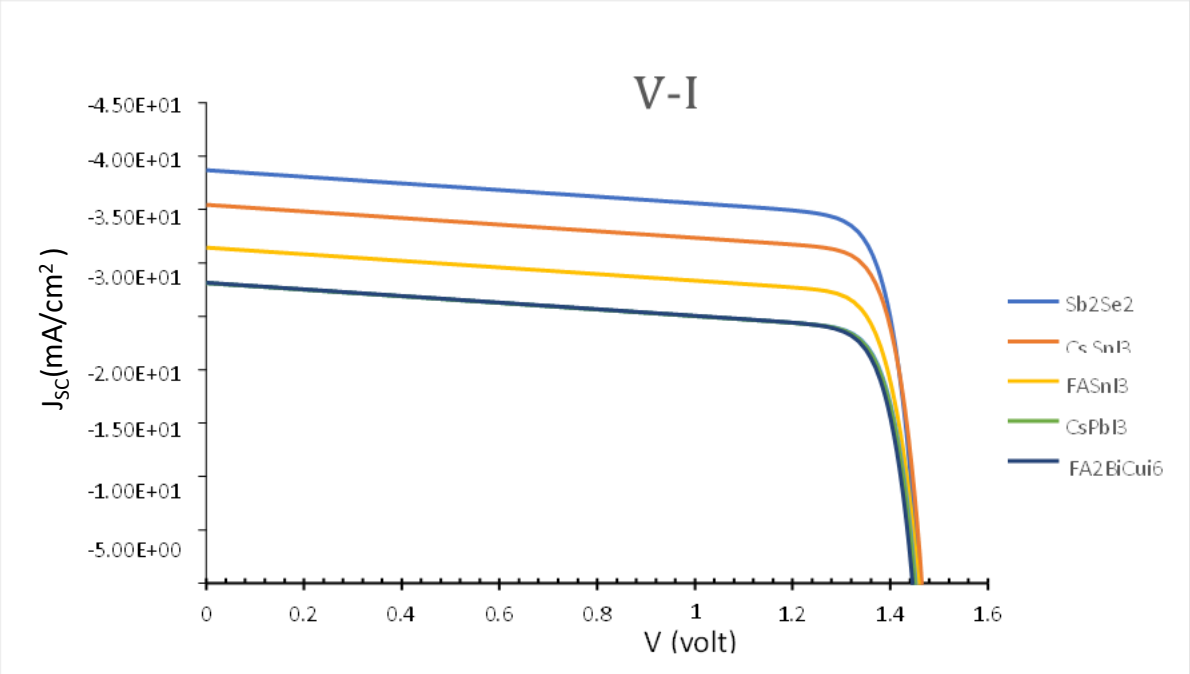

Figure 9 Curve Properties (I-V) After Adding Absorption Layer for Improved Cell

Figure 10 shows the improvement in the quantum efficiency curve, which now resembles a square shape, indicating an ideal case for quantum efficiency. Figure 11 represents the energy band diagram for the valence band and conduction band of the best absorption layer (Sb_2Se_3), which resulted in the highest conversion efficiency and quantum efficiency. The value of the conversion efficiency increased from 31.21% to 44.29% for the optimized cell. The reason behind this improvement is that the added layer acts as a selective barrier, allowing the transfer of electrons and holes from one side to another while reducing surface recombination [52]. As a result, the number of electron carriers on the surface increases, leading to improved solar cell performance.

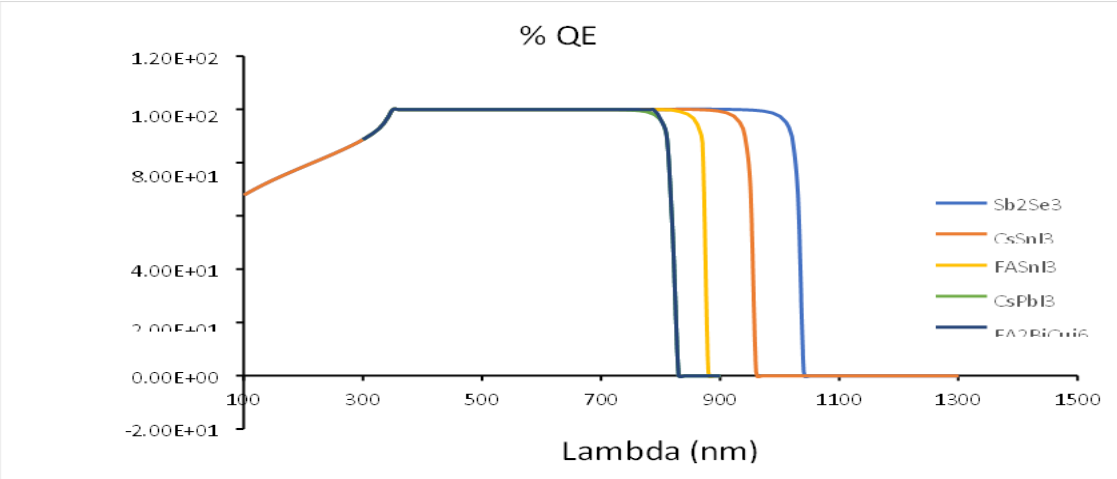

Figure 10 Curve Quantitative Efficiency After Adding Absorption Layer for Improved Cell

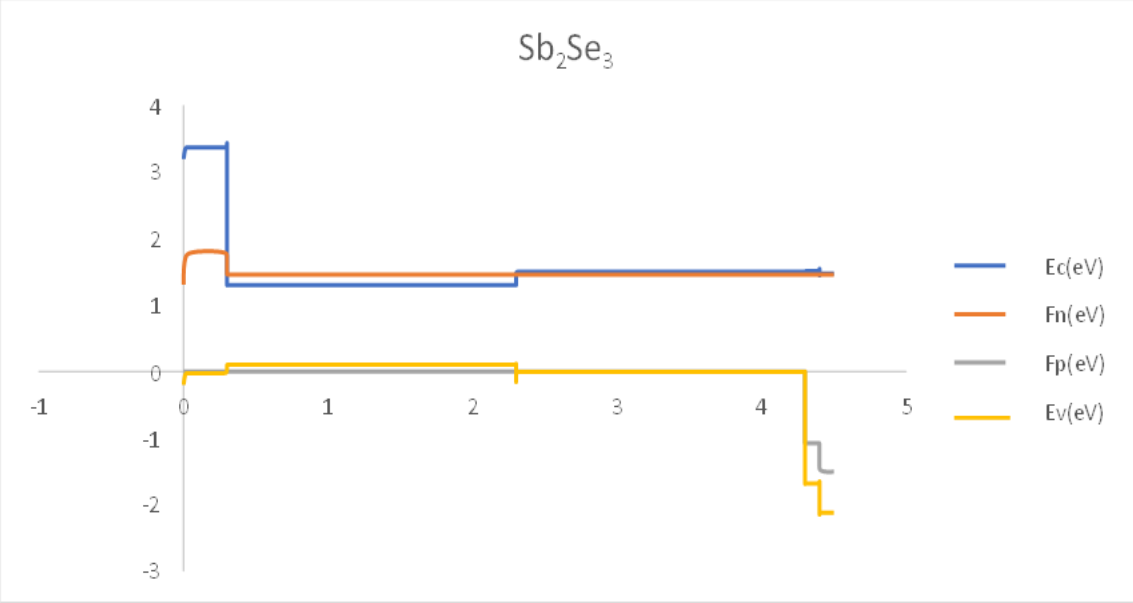

Figure 11 Energy Levels for Best Absorption Layer (Sb_2Se_3) for Improved Cell Conclusions

The efficiency of triformidinium-lead solar cells (FAPbI3) can be greatly improved by adding buffer layers and reflective layers

- Changing the buffer layer had a clear impact on the solar cell's performance, increasing it short-circuit current, open-circuit voltage, and fill factor. The best-performing layer was STO, achieving a conversion efficiency of 27.34%.
- Adding different back reflection layers to the solar cell improved its efficiency, with the CuScN layer giving the best results of 31.21% conversion efficiency.
- The study of the effect of a second layer found that adding a second layer between the back reflection layer and absorbing layer led to increased output values, with the solar cell using Sb_2Se_3 achieving a maximum conversion efficiency of 44.29%.

REFERENCES

1. Shaikh, S. F., Kwon, H. C., Yang, W., Mane, R. S., & Moon, J. (2018). Performance enhancement of mesoporous TiO2-based perovskite solar cells by ZnS ultrathin-interfacial modification layer. *Journal of Alloys and Compounds*, *738*, 405-414.
2. Eperon, G. E., Burlakov, V. M., Docampo, P., Goriely, A., & Snaith, H. J. (2014). Morphological control for high performance, solution-processed planar heterojunction perovskite solar cells. Advanced functional materials, 24(1), 151-157.
3. Liu, M., Johnston, M. B., & Snaith, H. J. (2013). Efficient planar heterojunction perovskite solar cells by vapour deposition. Nature, 501(7467), 395-398.
4. Sharma, R., Sharma, A., Agarwal, S., & Dhaka, M. S. (2022). Stability and efficiency issues, solutions and advancements in perovskite solar cells: A review. *Solar Energy*.
5. Gan, Y., Zhao, D., Qin, B., Bi, X., Liu, Y., Ning, W., ... & Jiang, Q. (2022). Numerical Simulation of High-Performance CsPbI3/FAPbI3 Heterojunction Perovskite Solar Cells. *Energies*, *15*(19), 7301.
6. Kanoun, M. B., Kanoun, A. A., Merad, A. E., & Goumri-Said, S. (2021). Device design optimization with interface engineering for highly efficient mixed cations and halides perovskite solar cells. *Results in Physics*, *20*, 103707.
7. Noman, M., Shahzaib, M., Jan, S. T., Shah, S. N., & Khan, A. D. (2023). 26.48% efficient and stable FAPbI 3 perovskite solar cells employing SrCu 2 O 2 as hole transport layer. *RSC advances*, *13*(3), 1892-1905.
8. Zhang, C., Wang, Y., Lin, X., Wu, T., Han, Q., Zhang, Y., & Han, L. (2021). Effects of A site doping on the crystallization of perovskite films. *Journal of Materials Chemistry A*, *9*(3), 1372-1394.
9. Wu, T., Qin, Z., Wang, Y., Wu, Y., Chen, W., Zhang, S., ... & Han, L. (2021). The main progress of perovskite solar cells in 2020–2021. *Nano-Micro Letters*, *13*, 1-18.
10. Al-Saqa, R. H., & Jassim, I. K. (2022). Effect of substrate temperature on the optical and structural properties of CaZnO3 perovskite thin films. *Journal of Nanomaterials & Biostructures*, *18*(1), 165-172.
11. Najim, A. H., & Saleh, A. N. (2019). Study effect of window and BSF layers on the properties of the CZTS/CZTSe solar cell by SCAPS–1D. *Tikrit Journal of Pure Science*, *24*(3), 77-83.
12. McCandless, B.; Hegedus, S. (1991). Photovoltaic Specialists Conference. *Solar EnergyMaterials and Solar Cells* .78(3). 967–972.
13. Zhen-Qi, L.; Ming, N. and Xiao-Dong, F. (2020). Simulation of the Sb2Se3 solar cell with a hole transport layer. Mater. Res. Express. 7(2) .016416.
14. Decock, K., Khelifi, S., & Burgelman, M. (2011). Modelling multivalent defects in thin film solar cells. *Thin Solid Films*, *519*(21), 7481-7484.
15. Al-Saqa, R. H., Jassim, I. K., & Uonis, M. M. (2023). Effect of KCl on the optical and structural properties of CaZnO 3 perovskite thin films. *Ochrona przed Korozją*, (8), 243-246.
16. Hameed, K. Y., Faisal, B., Hanae, T., Mari, S. B., Saira, B., & Kaim, K. N. A. (2019). Modelling of novel-structured copper barium tin sulphide thin film solar cells. *Bulletin of Materials Science*, *42*, 1-8.

17. Baig, F. (2019**).** Numerical analysis for efficiency enhancement of thin film solar cells .PhD,University Holand.
18. Kajal, M. P.; Fermi, H. I. & Joseph, J.P. (2018). Thickness optimization of CdS/ZnO hybrid buffer layer in CZTSe thin film solar cells using SCAPS simulation program. *Materials Research Innovations*.**12(7)**.231-235.
19. Burgleman et al, no May. 2014. SCAPS manual**,**
20. Ali, A. M., Alsaqa, R., & Sultan, N. S. (2022). Study of Thermodynamic Properties of Monoclinic Sulfur (Sβ) Under High Pressure Using Three Different Equations of State for the Treatment Scabies in Dermatology. *International Journal of Thermodynamics*, *25*(2), 33-38.
21. Karthick, S., Velumani, S., & Bouclé, J. (2020). Experimental and SCAPS simulated formamidinium perovskite solar cells: A comparison of device performance. *Solar Energy*, *205*, 349-357.
22. Guo, H.; Li, Y.;Guo, X.; Yuan, N. & Ding, J. (2018) .Effect of silicon doping on electrical and optical properties of stoichiometric Cu2ZnSnS4 solar cells **.***Physics B: Condensed Matter*. 531(4). 9-15.
23. Gan, Z., Zhao, L., Sun, X., Xu, K., Li, H., & Wei, J. (2022). Influence of Formamidine Formate Doping on Performance and Stability of FAPbI3-Based Perovskite Solar Cells. *Crystals*, *12*(9), 1194.
24. Mebarkia, C., Dib, D., Zerfaoui, H., & Belghit, R. (2016). Energy efficiency of a photovoltaic cell based thin films CZTS by SCAPS. *Journal of Fundamental and Applied Sciences*, *8*(2), 363- 371.
25. Al-saqa, Al-sheikh, (2013). Theoretical High pressure Study for Evaluation of Spinodal Pressure and Phonon Frequency Spectrum of Silver.
26. Raoui, Y., Ez-Zahraouy, H., Tahiri, N., El Bounagui, O., Ahmad, S., & Kazim, S. (2019). Performance analysis of MAPbI3 based perovskite solar cells employing diverse charge selective contacts:Simulation study. *Solar Energy*, *193*, 948-955.
27. Biswas, S. K., Sumon, M. S., Sarker, K., Orthe, M., & Ahmed, M. M. (2023). A Numerical Approach to Analysis of an Environment-Friendly Sn-Based Perovskite Solar Cell with SnO2 Buffer Layer Using SCAPS-1D. *Advances in Materials Science and Engineering*, *2023*.
28. Raoui, Y., Ez-Zahraouy, H., Tahiri, N., El Bounagui, O., Ahmad, S., & Kazim, S. (2019). Performance analysis of MAPbI3 based perovskite solar cells employing diverse charge selective contacts: Simulation study. *Solar Energy*, *193*, 948-955.
29. Hussain, S. S., Riaz, S., Nowsherwan, G. A., Jahangir, K., Raza, A., Iqbal, M. J., ... & Naseem,S. (2021). Numerical modeling and optimization of lead-free hybrid double perovskite solar cell by using SCAPS-1D. *Journal of Renewable Energy*, *2021*, 1-12.
30. McCandless, B.; Hegedus, S. (1991). Photovoltaic Specialists Conference. *Solar EnergyMaterials and Solar Cells* .78(3). 967–972.
31. Aleksandra, B;. Djuris,I. and Yu Hang, L. (2006). Optical Properties of ZnO Nanostructures *.small* . 2 (8-9), 944 – 961
32. Olopade, M. A., Oyebola, O. O., & Adeleke, B. S. (2012). Investigation of some materials as buffer layer in copper zinc tin sulphide (Cu2ZnSnS4) solar cells by SCAPS-1D. *Advances in Applied Science Research*, *3*(6), 3396-3400.

33. Tousif, M. N., Mohammad, S., Ferdous, A. A., & Hoque, M. A. (2018). Investigation of different materials as buffer layer in CZTS solar cells using SCAPS. *J. Clean Energy Technol*, *6*, 293-296.

34. Zhou, W. J., Jin, K. J., Guo, H. Z., He, X., He, M., Xu, X. L., ... & Yang, G. Z. (2015). Significant enhancement of photovoltage in artificially designed perovskite oxide structures. *Applied Physics Letters*, *106*(13).

35. AL-sheikh, A. M., & AL-Saqa, R. H. Evaluation of High-Pressure Effect of Phonon Frequency Spectrum for Gold by Using Different Equations of State (EOS). *Global Proceedings Repository, American Research Foundation, http://proceedings. sriweb. org ISSN*, *2476*, 58-278.

36. Najim, A. H.; & Saleh, A. N. (2019). Study effect of window and BSF layers on the properties of the CZTS/CZTSe solar cell by SCAPS–1D. *Tikrit Journal of Pure Science*.***24*(3)**. 77-83.

37. Chowdhury, T. A. (2023). Simulation Study of CuO-Based Solar Cell with Different Buffer Layers Using SCAPS-1D. *Energy and Power Engineering*, *15*(9), 307-314.

38. Emon, E. I., Islam, A. M., Sobayel, M. K., Islam, S., Akhtaruzzaman, M., Amin, N., ... & Rashid,M. J. (2023). A comprehensive photovoltaic study on tungsten disulfide (WS2) buffer layer based CdTe solar cell. *Heliyon*, *9*(3).

39. Naureen, Sadanand, Lohia, P., Dwivedi, D. K., & Ameen, S. (2022). A comparative study of quantum dot solar cell with two different ETLs of WS2 and IGZO using SCAPS-1D simulator. In *Solar* (Vol. 2, No. 3, pp. 341-353). MDPI.

40. Guo, H.; Li, Y.;Guo, X.; Yuan, N. & Ding, J. (2018) .Effect of silicon doping on electrical and optical properties of stoichiometric Cu2ZnSnS4 solar cells **.***Physics B: Condensed Matter*. 531(4). 9-15.

41. Büecheler S. F... (2010). Investigation of compound semiconductors as buffer-layer in thin film solar cells. PhD,University Zürich.

42. Kareem, S., Uonis, M., & Alsaqa, R. (2023). High-Pressure Calibration TiN Equation of State. *International Journal of Thermodynamics*, 1-7.

43. Mohammed, S. J. (2020). Simulation study of back surface and electron transport layers on Sb2Se3 solar Cell. *Tikrit Journal of Pure Science*, *25*(6), 103-113.

44. Li, Z. Q., Ni, M., & Feng, X. D. (2020). Simulation of the Sb2Se3 solar cell with a hole transport layer. *Materials Research Express*, *7*(1), 016416.

45. Rafee Mahbub, M., Islam, S., Anwar, F., Satter, S. S., & Ullah, S. M. (2016). Simulation of CZTS thin film solar cell for different buffer layers for high efficiency performance. *South Asian Journal of Engineering and Technology*, *2*(52), 1-10.

46. Zhen-Qi, L.; Ming, N. and Xiao-Dong, F. (2020). Simulation of the Sb2Se3 solar cell with a hole transport layer. Mater. Res. Express. 7(2) .016416.

47. Rau, U.; Schmidt, M.; Jasenek, A.; Hanna, G.; andSchock, H. W. (2011). Electrical Characterization Of Cu (In,Ga)Se2 Thin-Film Solar Cells and the Role of Defects for the Device Performance. *Solar EnergyMaterials and Solar Cells*. 67(4). 37-43

48. Saleh, M. M., Khemakhem, H., Jassim, I. K., & Al-Saqa, R. H. (2024). Structure and mechanical properties of cermet Ni-Al/MSZ thick coating prepared by flame spraying technique. *Ochrona przed Korozją*.

49. Sajid, S., Alzahmi, S., Salem, I. B., Park, J., & Obaidat, I. M. (2023). Lead-Free Perovskite Homojunction-Based HTM-Free Perovskite Solar Cells: Theoretical and Experimental Viewpoints. *Nanomaterials*, *13*(6), 983

50. Hussain, S. S., Riaz, S., Nowsherwan, G. A., Jahangir, K., Raza, A., Iqbal, M. J., ... & Naseem, S. (2021). Numerical modeling and optimization of lead-free hybrid double perovskite solar cell by using SCAPS-1D. Journal of Renewable Energy, 2021, 1-12.

51. Duha, A. U., & Borunda, M. F. (2022). Optimization of a Pb-free all-perovskite tandem solar cell with 30.85% efficiency. Optical Materials, 123, 111891

52. . Li, K., Wang, S., Chen, C., Kondrotas, R., Hu, M., Lu, S., ... & Tang, J. (2019). 7.5% n–i–p Sb2 Se 3 solar cells with CuSCN as a hole-transport layer. Journal of Materials Chemistry A, 7(16), 9665-9672